Dalton Transactions

ROYAL SOCIETY OF CHEMISTRY

PAPER

View Article Online
View Journal | View Issue

Cite this: *Dalton Trans.*, 2020, **49**, 187

A fluorescent "ON–OFF–ON" switch for the selective and sequential detection of Hg^{2+} and I^- with applications in imaging using human AGS gastric cancer cells†

Saswati Gharami,[a] Krishnendu Aich,[a] Paramita Ghosh,[b] Lakshman Patra,[a] Nabendu Murmu*[b] and Tapan K. Mondal*[a]

Received 2nd November 2019,
Accepted 18th November 2019

DOI: 10.1039/c9dt04245h

rsc.li/dalton

A new fluorescent "on–off–on" probe (BIPQ) is designed and developed which selectively binds with Hg^{2+}; its emission intensity is quenched almost 40-fold at 455 nm without interference from other metal cations. On gradual addition of I^- to the solution of BIPQ-Hg^{2+}, the emission reverts to its original intensity. The limits of detection of BIPQ for Hg^{2+} and I^- are found to be on the order of 3.12×10^{-9} and 5.48×10^{-8} M, respectively, which shows clearly that BIPQ can sense Hg^{2+} at a very minute level. DFT and TDDFT studies are conducted with the probe to establish similarity between theoretical and experimental outcomes. Finally, to demonstrate its practical benefit in biological fields, live cell imaging experiments with BIPQ are carried out to detect Hg^{2+} in human AGS gastric cancer cell lines.

Introduction

In current research, the design, development and implementation of fluorescent chemosensors has recently gained massive interest due to their specific and nondestructive responses as well as their facile monitoring of bioactive cations and anions in different biological, environmental, toxicological and industrial samples. They are also useful in molecular devices, nerve gas sensors, *etc*.[1,2] The precise fluorescence responses of these chemosensors have received a great deal of attention due to their easy-to-handle characteristics, low cost and rapid discovery of target analytes.[3] The developed chemosensors show specific sensing towards their target molecules *via* quenching, enhancing or ratiometric shifting of their emission maxima, which facilitates rapid detection. The detection of toxic heavy metal ions has recently become very important due to their high accumulation in water and food, which frequently leads to various dangerous diseases in living beings.[4] Among all cations and anions, Hg^{2+} is one of the most detrimental and widespread heavy metal ions found in our flora and fauna.[5] Mercury, which is known to be a 'liquid metal' in its native form, can cause permanent damage to DNA and the nervous system if exposed or inhaled in high quantity.[6] The Environmental Protection Agency (EPA) has set a maximum allowable level of 2 ppb (10 nM) for mercury contamination in food and drinking water.[7] Inorganic mercury can be converted to methyl mercury by bacteria; this substance can bioaccumulate in the food chain[8] as well as in the human body, leading to various cognitive and motor disorders along with pulmonary edema, cyanosis, nephritic syndrome and Minamata disease.[9] Thus, there is still high demand for mercury detection methodologies for sensitive and appropriate recognition as well as hazardous assessment. Therefore, it is highly desirable to develop a powerful and sensitive analytical tool for the detection of Hg^{2+} in environmental samples. There are few reports of fluorescent probe-Hg^{2+}-ensembles that sense iodide.[10–27] Among biologically significant anions, iodide is one of the most important because it is a vital micronutrient that plays essential physiological roles in human development.[28] Specifically, excessive iodine intake as well as deficiency can lead to thyroid disease because iodine plays an essential role in thyroid gland function.[29] Low iodine intake generally results in hypothyroidism, endemic goiter cretinism, congenital anomalies, neurological disorders and intellectual disability.[30–35] Iodine also exhibits anti-inflammatory and anti-oxidative activities.[36] Moreover, elemental iodine has often been used in numerous areas of chemistry for synthesizing drugs, dyes, *etc*. Generally, reported chemosensors are

[a]*Department of Chemistry, Jadavpur University, Kolkata-700032, India. E-mail: tapank.mondal@jadavpuruniversity.in*
[b]*Department of Signal Transduction and Biogenis Amines (STBA), Chittaranjan National Cancer Institute, Kolkata-700026, India. E-mail: nabendu.murmu@cnci.org.in*

†Electronic supplementary information (ESI) available: NMR and MS of all new compounds, limit of detection determination, quantum yield calculation *etc*. CCDC 1914359. For ESI and crystallographic data in CIF or other electronic format see DOI: 10.1039/C9DT04245H

designed to recognize metal cations.[37–42] However, in the case of anion recognition, the detection of iodide is somewhat less reported, and its bio-imaging studies have also received less focus, probably due to their low solubility and selectivity.[43,44] However, developing a fluorescent probe-metal ensemble to selectively bind targeted anions is an efficient method of anion detection. The ensemble shows 'turn-on' fluorescence enhancement for anion detection because it is non-fluorescent itself. A few successful fluorescent probes have been reported to date which can selectively detect iodide ion.[45–47] However, only a few optical sensors have been reported for selective detection of iodide in aqueous systems due to the heavy atom effect of iodide, thereby leading to weak interactions of the fluorescent probes with the target anions.[48–53] Therefore, it remains a highly desirable task to design a fluorescent probe which recognizes both Hg^{2+} and I^- simultaneously with low detection limit values.

In 2013, Zhang *et al.* reported a quinoline-based probe (HL) which shows "turn-off" fluorescence quenching response towards Hg^{2+}, and the Hg^{2+}-HL compound showed emission enhancement upon addition of CN^-.[21] Again in 2019, Ali *et al.* reported a fluorescein-based chemosensor which showed a "turn-on" emission upon Hg^{2+} addition with a detection limit of 1.24 μM; upon addition of S^{2-}, it displayed a "turn-off" response.[22] Chen *et al.* recently reported a pyrene-functionalized norbornene and its homopolymer, which showed ratiometric sensing towards Hg^{2+}; in turn, it could detect biothiols, including cysteine, by forming an *in situ* Hg^{2+}-complex with the probe.[17] The limit of detection for Hg^{2+} was found to be 38.3 nM, which is quite high. Chang and co-workers reported a quinoline-based fluorescent probe in 2006 which also showed fluorescence enhancement properties upon addition of Hg^{2+} with a LOD value of 540 nM.[23] Further, in 2019, Yang *et al.* designed a pyrazole-based probe which showed a "turn-on" fluorescence change upon addition of Hg^{2+} in DMSO : H_2O (1/1, v/v) solvent with a detection limit of 20.7 nM.[24] In the same year, Rashatasakhon and co-workers reported a spirobifluorene derivative-based probe which showed quenching of its emission intensity in the presence of Hg^{2+} in DMSO solvent with a detection limit of 10.4 to 103.8 nM.[25] Again in 2011, Tsukamoto *et al.* published a coumarin-based fluorescence switch with "turn-on" emission properties towards both Hg^{2+} and Ag^+ in phosphate buffer containing 0.1% DMSO solvent.[26] The detection limit of the probe was found to be 2 ppb for Hg^{2+}. Sivaraman's group developed two phosphonate-based fluorescent ratiometric probes in 2019 which detect Hg^{2+} selectively in MeOH/H_2O (7/3, v/v) solvent with LOD values of 865 nM and 372 nM.[27] Now, in the present report, we have designed a relatively simple-to-synthesize quinoline-based fluorescent probe (BIPQ) which shows a quenching effect in the presence of Hg^{2+} in MeOH/H_2O (1/4, v/v) solvent and reverts to the original intensity on addition of 2 equivalents of I^-. The detection limit was observed to be 3.12 nM for Hg^{2+}, which is a sufficiently low LOD value; moreover, the single crystal X-ray structure of BIPQ-Hg^{2+} was studied and confirmed the exact binding mode of Hg^{2+} with BIPQ. A live cell imaging experiment of BIPQ was also executed, and the results indicate that BIPQ can be used as a bio-marker in human AGS cells for detecting Hg^{2+} as well as I^-, thereby establishing the application part of the probe in the biological field.

On the other hand, in the field of anion receptors, a few reports on the development of iodide sensors have been noted. As an example, in 2012, Beer's group reported two macrocycles containing naphthalene moieties, among which one probe selectively binds with I^-, showing an increase in emission intensity; meanwhile, in that same year, Martínez-Máñez and co-workers fabricated hybrid silicananoparticle-based fluorogenic moieties with imidazolium groups as anion coordination sites which showed specific emission responses towards iodide and benzoate anions.[48] Currently, the synthesis and design of these iodide sensors are somewhat complicated; meanwhile, in the present case, BIPQ-Hg^{2+} can be easily achieved *in situ*, and the detection of I^- using this system is also very effective. Consequently, we can detect both Hg^{2+} and I^- sequentially using this probe (BIPQ).

Experimental section

Reagents and physical measurements

All reagents and solvents used in the synthesis were purchased from Aldrich. Elemental analysis was carried out in a 2400 Series-II CHN analyzer, PerkinElmer, USA. Thin layer chromatography (TLC) was performed using Merck 60 F254 plates with a thickness of 0.25 mm. $CDCl_3$ and DMSO-d_6 were used as solvents and TMS was used as an internal standard for the NMR spectra. ^1H and ^{13}C NMR spectra were recorded on a Bruker 300 MHz instrument. Chemical shifts are denoted by δ units and ^1H–^1H and ^1H–C coupling constants are expressed in Hz. HRMS mass spectra were recorded on a Waters (Xevo G2 Q-TOF) mass spectrometer. UV-vis spectra were acquired on a PerkinElmer Lambda 750 spectrophotometer. The fluorescence properties were measured using a Shimadzu RF-6000 fluorescence spectrophotometer at room temperature (298 K), and fluorescence lifetimes were measured using a time-resolved spectrofluorometer from IBH, UK.

Synthesis of 2-(1*H*-benzo[*d*]imidazol-2-yl)quinolin-8-ol (1)

8-Hydroxyquinoline-2-carbaldehyde (0.25 g, 1.44 mmol) and *o*-phenylenediamine (0.16 g, 1.44 mmol) were taken in a round-bottomed flask and dissolved in DMF (5 mL) solution, followed by the addition of a catalytic amount of p-TSA (~15 mg). Then, the mixture was refluxed for 4 hours under inert atmosphere. After completion of the reaction, the reaction mixture was cooled at room temperature; then, the whole mixture was poured into ice-cold water, followed by the formation of a light yellow precipitate. The precipitate was filtered and subjected to column chromatography using an ethyl-acetate-petroleum ether mixture as the eluent to afford a deep yellow solid compound. The yield was 0.32 g (84%). The compound was sufficiently pure to be used directly in the next step to yield the desired probe.

^{1}H NMR (300 MHz, $CDCl_3$): δ 7.27 (d, J = 7.8 Hz, 2H), 7.42 (d, J = 8.2 Hz, 1H), 7.62 (t, J = 7.9 Hz, 1H), 8.05 (d, J = 8.2 Hz, 2H), 8.15 (s, 1H), 8.31 (d, J = 8.2 Hz, 1H), 10.21 (s, 1H), 13.31 (S, 1H).

HRMS: calculated for $C_{16}H_{12}N_3O$ $[M + H]^+$ (m/z): 262.0983; found: 262.1707.

Synthesis of 2-(1*H*-benzo[*d*]imidazol-2-yl)-8-(pyridin-2-ylmethoxy)quinoline (BIPQ)

To a solution of compound **1** (0.10 g, 0.39 mmol) in DMF (5 mL), K_2CO_3 (0.13 g, 0.79 mmol) was added, and the mixture was stirred for about 10 min at room temperature. Then, 2-(chloromethyl)pyridine hydrochloride (0.08 g, 0.48 mmol) was added to the reaction mixture followed by the addition of catalytic amounts of KI and tetra-*n*-butylammonium bromide (TBAB), and the stirring was continued for 8 h at room temperature under nitrogen atmosphere. After monitoring by TLC and confirming the formation of the desired product, the whole reaction mixture was cooled, poured into ice water and then extracted using dichloromethane (3 × 20 mL). Then, the DCM segment was dried over anhydrous sodium sulphate and evaporated. Evaporation of the solvent under reduced pressure afforded a solid compound which was purified through column chromatography using ethylacetate-petroleum ether as the eluent to yield BIPQ (0.12 g, 88%) as a light yellow solid.

^{1}H NMR (300 MHz, $CDCl_3$): δ 5.31 (s, 2H), 6.71 (s, 1H), 7.04–7.08 (m, 1H), 7.12–7.20 (m, 1H), 7.29–7.36 (m, 1H), 7.42–7.46 (m, 1H), 7.54–7.62 (m, 1H), 7.87 (d, J = 7.6 Hz, 1H), 8.00 (s, 1H), 8.27 (d, J = 8.4 Hz, 1H), 8.51–8.60 (m, 1H), 8.70 (d, J = 8.6 Hz, 1H), 12.92 (s, 1H). **^{13}C NMR (75 MHz, $CDCl_3$):** δ 72.6, 110.0, 111.2, 112.6, 119.8, 121.0, 122.2, 122.6, 123.0, 123.9, 127.6, 129.8, 136.7, 137.2, 148.9, 151.2, 154.0, 157.6.

HRMS: Calculated for $C_{22}H_{17}N_4O$ $[M + H]^+$ (m/z) = 353.1402; found = 353.0544.

Synthesis of BIPQ-Hg^{2+} complex

The probe BIPQ (55 mg) and $HgCl_2$ (42 mg) were mixed and dissolved in 8 mL of methanol, and the mixture was refluxed for 2 hours. After completion of the reaction, the reaction mixture was cooled to room temperature; a light brownish precipitate appeared and was filtered and dried. Single brown crystals of the complex were obtained by slow diffusion of *n*-hexane into DCM solution. The yield of the complex was 0.084 g (86%).

^{1}H NMR (300 MHz, DMSO-d_6): δ 5.63 (s, 2H), 7.37 (m, 4H), 7.49–7.60 (m, 1H), 7.65–7.71 (m, 2H), 7.80 (m, 3H), 8.54 (d, J = 8.5 Hz, 1H), 8.59 (s, 1H), 8.71 (d, J = 8.5 Hz, 1H).

HRMS: Calculated for $C_{22}H_{16}N_4OCl_2Hg$ $[M + H]^+$ (m/z): 624.0396; found: 624.1373.

Live cell imaging studies

Cell cytotoxicity assay. Gastric cancer (AGS) cells were used to study the cytotoxicities of mercury chloride (Hg^{2+}), BIPQ and BIPQ in the presence of Hg^{2+} and I^- complexes. The cells were incubated in 96-well plates, where each well contained a cover slip at the bottom, at a density of 5 × 10^3 cells per well and cultured in a CO_2 incubator for 24 h at 37 °C. The cells were incubated with incremental doses (0, 10, 50, 75, 100, 150, 200, 250, 300 μM) of free BIPQ and $HgCl_2$ separately along with controls for 24 h. Then, the residual probe and Hg^{2+} were washed with PBS. After 24 h treatment, the cover slip was removed and methyl tetrazolium dye (MTT) (5 mg ml^{-1}) solution was added to each well plate (10 μl per well) for 2 h in the dark. Next, the cell viability was estimated by recording the absorbance at 570 nm for each well using a microplate reader (Tecan, infinite M200). Hg^{2+} was obtained by dissolving $HgCl_2$ in aqueous medium, while the probe (BIPQ) was dissolved in DMSO; the final concentration of DMSO while treating the cells was preserved below 1%. The untreated cells were treated as 100% viable. The plot of a non-linear regression curve between the log of the concentration of BIPQ and the O.D. value at 570 nm was drawn to determine the IC_{50} value of BIPQ.

Cell bio imaging. AGS cells were grown on 22 × 22 mm glass cover slips which were placed at the bottom of 12-well plates overnight. Then, the cells were treated with BIPQ (15 μM) for 1 h. The amount of BIPQ was chosen based on the IC_{50} value, which was determined to be 185.1 μM. After the experiment, the cells were fixed with methanol and washed with 0.5% phosphate buffer saline tween (PBS) twice, then with 1 × PBS thrice. Subsequently, they were treated with Hg^{2+} (30 μM) for another 30 minutes and washed three times with 0.5% phosphate buffer saline tween (PBS). Fluorescence images of the cells treated with BIPQ and BIPQ-Hg^{2+} were observed under a fluorescence microscope (Leica DM4000 B, Germany) at 20× magnification. Further, the cells treated with BIPQ-Hg^{2+} were incubated for 1 h in the presence of 30 μM KI solution and again observed through a fluorescence microscope.

Theoretical studies. All calculations were performed with the Gaussian 09 program package.[54] Full geometry optimizations of BIPQ and BIPQ-Hg^{2+} were carried out using the density functional theory (DFT) method at the B3LYP[55,56] level. The 6-31+G(d) basis set was assigned for all the elements except Hg^{2+}. The LanL2DZ basis set with the effective core potential set of Hay and Wadt[57] was used for mercury. Vertical electronic excitations based on B3LYP optimized geometries were computed using the time-dependent density functional theory (TDDFT) formalism[58–60] in methanol using the conductor-like polarizable continuum model (CPCM).[61–63]

Results and discussion

Synthesis of the probe (BIPQ)

Compound **1** was synthesized *via* simple reflux condensation of *o*-phenylenediamine and 8-hydroxyquinoline-2-carbaldehyde in DMF solution with a yield of 84%; it was then used in the next step. Therefore, the synthesis of our probe, BIPQ, involved stirring compound **1** and 2-(chloromethyl)pyridine hydrochloride (2) in DMF at room temperature with addition of K_2CO_3 and a pinch of TBAB (Scheme 1). The yield was 88%. The structures of BIPQ and BIPQ-Hg^{2+} were confirmed by ^{1}H

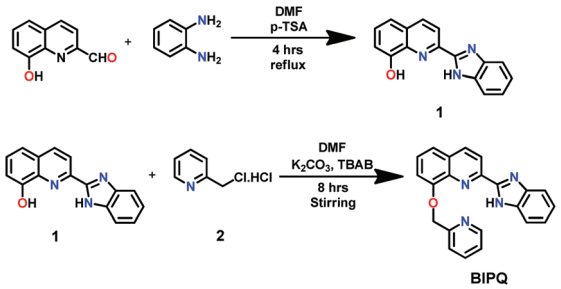

Scheme 1 Synthetic scheme for the probe BIPQ.

and ^{13}C NMR spectroscopy and ESI mass spectrometry (ESI, Fig. S1–S7†).

Photophysical studies of BIPQ

The sensing properties of BIPQ, including its absorbance and emission properties, were studied in methanol–water (1/4, v/v) solution at 25 °C at physiological pH (10 mM HEPES buffer, pH 7.4) in the presence of different analytes.

UV-Vis studies

The absorption spectral changes of BIPQ were recorded upon gradual addition of different metal cations. The solution of BIPQ (10 μM) in MeOH/H_2O (1/4, v/v) shows a peak at 292 and 337 nm in the absence of other metal ions. Upon gradual addition of Hg^{2+} to the solution of BIPQ, the band at 292 nm decreases, whereas the band at 337 nm shows a slight red shift and a new peak at 355 nm is observed. As a result, three distinct isosbestic points are noted at 267 nm, 309 nm and 345 nm, respectively (Fig. 1a). To ascertain the selectivity of the probe to mercury, the absorption spectral changes of the probe in the presence of other metal cations were also recorded; the results confirmed that no red shift of the aforementioned absorption band of BIPQ was observed in the presence of any metal cations except Hg^{2+} (ESI, Fig. S9†). Upon gradual addition of I^- to this BIPQ-Hg^{2+} solution, the band at 292 nm reappears and the peak at 355 nm vanishes as the original band at 337 nm returns (Fig. 1b). These changes in the absorption spectra of BIPQ-Hg^{2+} were also recorded in the presence of other anions, such as Br^-, F^-, NO_2^-, NO_3^-, S^{2-}, PO_4^{3-}, SO_4^{2-}, SO_3^{2-}, Cl^- and N_3^-. However, it was noted that in the presence of other anions, the absorption changes of BIPQ-Hg^{2+} cannot return to the original absorption of BIPQ, thereby clearly indicating that no anions except I^- cause any significant changes in the absorption of BIPQ-Hg^{2+} (ESI, Fig. S10†).

Fluorescence studies

Emission studies of BIPQ were also carried out in a mixed aqueous solution, *i.e.*, MeOH/H_2O (1/4, v/v) solution, in the presence of other metal ions. BIPQ exhibits a very strong emission band (ϕ = 0.56) at 455 nm in MeOH/H_2O (1/4, v/v) solution upon excitation at 340 nm. After incremental addition of Hg^{2+} to the solution of the probe, the peak of BIPQ at 455 nm is sharply quenched, with a red shift of almost 30 nm (Fig. 2a). Consequently, a change is noted in the emission color after irradiation with UV-light. The probe solution, which was observed to be cyan, became colorless after addition of Hg^{2+} (Fig. 2a, inset). The new maximum of BIPQ-Hg^{2+} appears at 485 nm. To assess its specific selectivity profile towards Hg^{2+}, other metal ions, such as Na^+, K^+, Co^{2+}, Ni^{2+}, Cu^{2+}, Cd^{2+}, Mn^{2+}, Al^{3+}, Ca^{2+}, Cr^{3+}, Fe^{3+}, Mg^{2+}, Pb^{2+}, Au^{3+} and Ag^+, were chosen as competing ions; it was established that no metal ions other than Hg^{2+} caused any significant quenching impact in the emission profile of BIPQ (Fig. 3a).

We also investigated the emission profile of compound **1** (10 μM) in MeOH/H_2O (1/4, v/v) solution. Compound **1** showed very weak fluorescence at 447 nm upon excitation at 350 nm.

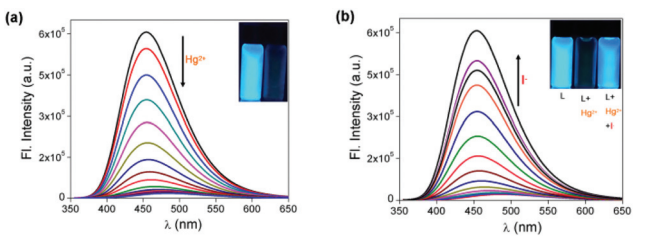

Fig. 2 Changes in the emission spectra of (a) BIPQ (10 μM) upon addition of Hg^{2+} (0 to 20 μM) and (b) changes in the UV-Vis spectra of BIPQ-Hg^{2+} upon addition of I^- (0 to 20 μM) in MeOH/H_2O (1/4, v/v) (10 mM HEPES buffer, pH 7.4). (The insets show the changes in colour under the UV-light.).

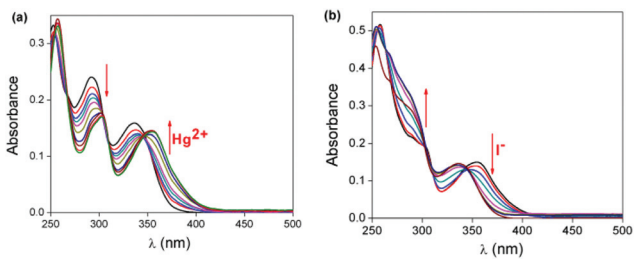

Fig. 1 Changes in the UV-Vis spectrum of (a) BIPQ (10 μM) upon addition of Hg^{2+} (0 to 20 μM) and (b) changes in the UV-Vis spectrum of BIPQ-Hg^{2+} upon addition of I^- (0 to 20 μM) in MeOH/H_2O (1/4, v/v) (10 mM HEPES buffer, pH 7.4).

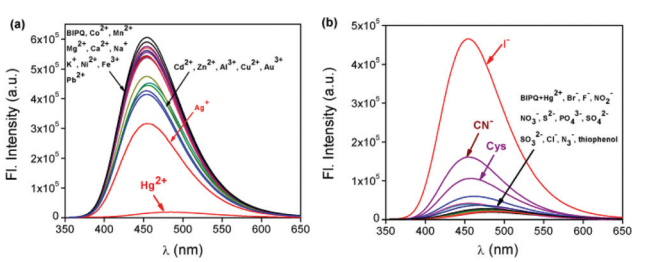

Fig. 3 Changes in emission intensity of (a) BIPQ (10 μM) upon addition of different metal ions (20 μM) in MeOH/H_2O (1/4, v/v) and of (b) BIPQ-Hg^{2+} upon addition of different anions (20 μM) in MeOH/H_2O (1/4, v/v) (10 mM HEPES buffer, pH 7.4).

After adding 20 μM of Hg^{2+} solution, the emission intensity was further quenched. Now, this *in situ* compound **1**-Hg^{2+} complex solution displayed slight enhancement of its emission intensity upon addition of 20 μM of I^- solution (ESI, Fig. S11†). Because the emission response did not exhibit any significant changes, further studies were not performed with compound **1**.

BIPQ-Hg^{2+} solution shows an enhancement in emission intensity in the presence of I^-. With gradual addition of I^- to the BIPQ-Hg^{2+} solution, the emission intensity at 485 nm actually reverts to the original emission intensity of BIPQ at 455 nm (Fig. 2b). As a result, the colorless solution of BIPQ-Hg^{2+} is converted to the previous cyan color when irradiated with UV light; this proves that the probe BIPQ is freed from complexation with mercury due to the formation of HgI_2. This emission change of BIPQ-Hg^{2+} to its original intensity was also recorded in the presence of other anions, *i.e.*, Br^-, F^-, NO_2^-, NO_3^-, S^{2-}, PO_4^{3-}, SO_4^{2-}, SO_3^{2-}, Cl^-, N_3^-, CN^-, cysteine and thiophenol (Fig. 3b). Although CN^- showed some extent of fluorescence enhancement when added to the BIPQ-Hg^{2+} solution, the change was not as significant as that obtained with I^-. The excellent quenching of the emission intensity of BIPQ may be due to the chelation enhancement quenching effect (CHEQ). Therefore, the BIPQ-Hg^{2+} assembly can act as a potentially selective and reversible fluorescent probe for I^- in the presence of other competing anions at physiological pH.

The emission intensity of the switch (BIPQ) at 485 nm decreased linearly with increasing amount of added Hg^{2+} in the range of 0 to 7 μM, with a good R^2 value of 0.9956 (ESI, Fig. S12a†). The limit of detection of BIPQ for Hg^{2+} was determined from the fluorescence spectral changes upon addition of Hg^{2+}; it was found to be 3.12×10^{-9} M (ESI, Fig. S13a†). On the other hand, for I^-, the emission intensity of BIPQ increased linearly at 455 nm in the range of 0 to 7 μM (R^2 = 0.9821) (ESI, Fig. S12b†), and the detection limit was calculated to be 5.48×10^{-8} M (ESI, Fig. S13b†). The LOD values clearly demonstrate that BIPQ can efficiently detect Hg^{2+} in a very minute amount, while BIPQ-Hg^{2+} is also very efficient in sensing I^-.

Next, in order to quantify the stoichiometry of the complex of BIPQ with Hg^{2+}, Job's plot analysis was carried out. The maximum appears at a mole fraction of 0.5 for mercury, which corresponds to the formation of a 1 : 1 complex of BIPQ and Hg^{2+} (ESI, Fig. S14†). The association constant (K_a) of BIPQ for Hg^{2+} was determined to be 1.4×10^6 M^{-1} from the Benesi–Hildebrand plot using the data obtained from fluorescence titration (ESI, Fig. S15†). The association constant value indicates that the BIPQ-Hg^{2+} complex moiety is stable enough. The HRMS of BIPQ shows a peak at *m*/*z* 353.0544, probably for $[BIPQ + H]^+$ (ESI, Fig. S5†), whereas the Hg^{2+} complex exhibits peaks at *m*/*z* 624.1373, respectively, accounting for the possible composition $[BIPQ + Hg^{2+} + H]^+$; this confirms the formation of a mononuclear complex of BIPQ with Hg^{2+} (ESI, Fig. S7†) (Scheme 2).

We studied ^1H NMR titration of the probe (BIPQ) upon addition of 2 equivalents of Hg^{2+} in DMSO-d_6 solvent. From the NMR data, it was observed that the –NH peak arises at δ 12.92 ppm and disappears upon addition of Hg^{2+}; also, the $-CH_2$ proton is observed to have a slight downfield shift due to the binding of its corresponding O-atom to Hg^{2+}. All the other aromatic protons also experienced slight downfield shifts. Therefore, this ^1H NMR titration study clearly ascertained that the amine proton takes part in the binding of BIPQ with Hg^{2+} (Fig. S8†).

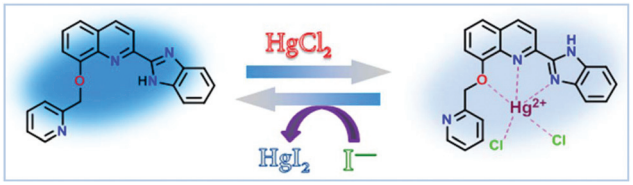

Scheme 2 Proposed schematic of the sensing mechanism.

To comprehend the excited state stability, fluorescence lifetime measurements were also carried out. The lifetime decays of the free probe (BIPQ) show mono-exponential decay, whereas the BIPQ-Hg^{2+} complex as well as BIPQ-Hg^{2+}-I^- fit well with the bi-exponential decay curve. The lifetime of BIPQ (12.82 ns) is significantly decreased in the presence of Hg^{2+} (1.28 ns) due to the complexation of BIPQ with mercury, whereas on addition of I^-, the lifetime again increased to 9.66 ns (ESI, Fig. S16†).

An interference experiment was carried out by measuring the emission intensity of BIPQ (10 μM) in the presence of other metal cations (20 μM) in order to study the selectivity of the probe. It was observed that the fluorescence quenching of BIPQ is specific towards only Hg^{2+} (ESI, Fig. S17a†) and is not affected by the presence of other metal cations. A similar experiment was performed on BIPQ-Hg^{2+} in the presence of other anions, and it was observed that the emission intensity of the aforementioned moiety increases only in the presence of I^-; no significant changes can be noted for other anions except Cl^- and N_3^- (ESI, Fig. S17b†).

pH studies

The effects of pH on the emission spectrum of BIPQ were demonstrated in the absence and presence of Hg^{2+} and I^- at 455 nm. The study clearly reveals that BIPQ undergoes a sharp change in emission intensity at pH 4 and shows a saturated increase in the pH range of 5 to 12, suggesting that the probe is sufficiently stable in this pH range. On addition of Hg^{2+} to the solution of BIPQ, the emission intensity decreases rapidly within the pH range of 2 to 8; this establishes that BIPQ can efficiently detect Hg^{2+} within the aforementioned pH range (Fig. 4). Further, in the pH range of 9 to 12, the emission intensity increases slightly on addition of Hg^{2+} due to the dissociation of BIPQ-Hg^{2+} in this basic pH range. Similarly, on addition of I^- to the BIPQ-Hg^{2+} solution, the emission intensity again increases with increasing pH and shows almost the same profile as in the case of BIPQ. Hence, the BIPQ-Hg^{2+} switch can detect I^- in the neutral pH range with brilliant efficiency.

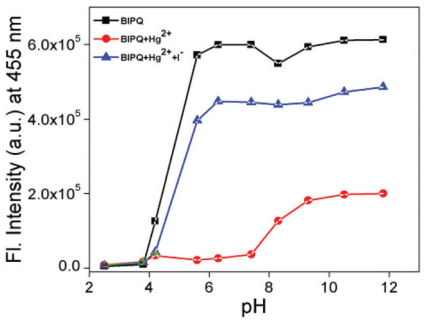

Fig. 4 pH studies of BIPQ, BIPQ-Hg^{2+} and BIPQ-Hg^{2+}-I^-.

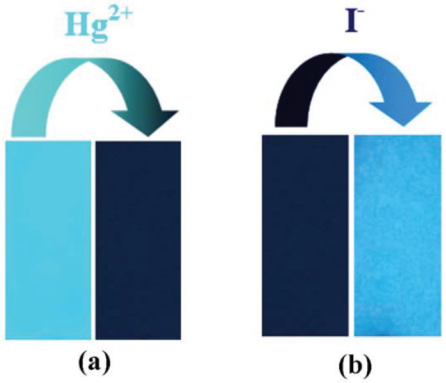

Fig. 5 Photographs of TLC plates after immersion in BIPQ-methanol solution and after immersion in (a) BIPQ-Hg^{2+} and (b) BIPQ-Hg^{2+}-I^- methanol solutions under hand-held UV light. The excitation wavelength of the UV light is 340 nm. [BIPQ] = 2×10^{-4} M, [Hg^{2+}] and [I^-] = 2×10^{-3} M.

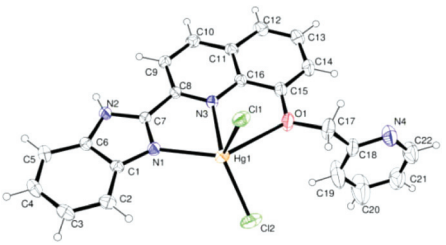

Fig. 6 ORTEP of BIPQ-Hg^{2+} with 35% ellipsoidal probability.

Computational studies

We carried out DFT calculations to study the structural changes of BIPQ in the presence of Hg^{2+} using the B3LYP/6-31+G(d) method with the Gaussian 09 program. The optimized structures of BIPQ and BIPQ-Hg^{2+} are shown in Fig. S18 and S19,† respectively. The HOMO–LUMO energy gap of BIPQ is 3.94 eV, which is significantly diminished in the BIPQ-Hg^{2+} (3.74 eV) complex; this indicates shifting of the low energy band in the complex, leading to the formation of a new band at a longer wavelength after addition of Hg^{2+} to the BIPQ solution, *i.e.*, due to BIPQ-Hg^{2+} complex formation. The energy and % compositions of selected molecular orbitals of BIPQ-Hg^{2+} are summarized in Table S1.† Further, to infer the electronic transitions of BIPQ and its mercury complex, time-dependent density functional theory (TDDFT) studies were conducted to determine the optimized geometries of the compounds. The low energy transition for BIPQ at 357 nm ($\lambda_{expt.}$, 337 nm) corresponds to the HOMO → LUMO transition, whereas for BIPQ-Hg^{2+}, the low energy band shifted to 380 nm ($\lambda_{expt.}$, 355 nm) (Table S2†). The contour plots of selected molecular orbitals, including the HOMO and LUMO of BIPQ and BIPQ-Hg^{2+}, are also shown in Fig. S20 and S21,† respectively.

Test kit for the detection of Hg^{2+} and I^-

The instant response of the switch BIPQ towards Hg^{2+} and I^- suggests its potential application for use as a neat portable kit for sensing the abovementioned analytes. In order to investigate the practical use of this newly developed fluorescent switch, the dip-stick method has been proved to be a simple but very important experiment. Therefore, a few thin-layer chromatography (TLC) plates were prepared, then soaked in a solution of BIPQ (2×10^{-4} M) in methanol and then allowed to dry for a few minutes. Then, the TLC plates were dipped into Hg^{2+} solution (2×10^{-3} M) and allowed to evaporate again. These dried TLC plates were again dipped into I^- solution (2×10^{-3} M), and the solvent was evaporated to allow them to dry. The colour of the TLC plates shows a change from cyan to colorless in the case of Hg^{2+} under UV light and from colorless to cyan for I^- (Fig. 5).

Crystallographic studies

The structure of BIPQ-Hg^{2+} was further determined by single crystal X-ray diffraction. The ORTEP plot and atom numbering scheme of the complex BIPQ-Hg^{2+} are shown in Fig. 6. BIPQ acts as a tridentate N,N,O donor ligand in the complex. The metal is coordinated with BIPQ through an imidazole nitrogen atom (N1), pyridyl nitrogen atom (N3) and ether oxygen atom (O1) *via* formation of two five-membered (Hg1–N1–C7–C8–N3) and (Hg1–O1–C15–C16–N3) chelate rings with chelate bite angles <N1–Hg1–N3 and <N3–Hg1–O1 of 71.51(7)° and 62.57(6)°, respectively. Selected bond distances and bond angles of BIPQ-Hg^{2+} are given in Table S4.† The M–N (imidazole) bond distance, Hg1–N1 (2.293(2) Å), is significantly shorter than the M–N (pyridyl) bond distance, Hg1–N3 (2.407(2) Å), in the complex. The Hg–O (ether) bond distance was found to be much longer, Hg1–O1 (2.7161(19) Å), as expected. In the complex, the geometry around Hg(II) is square pyramidal, as indicated by the value of the trigonal index τ = 0.005 ($\tau = (\beta - \alpha)/60$), where α and β are the largest coordination angles. The value of τ is 1 for a perfect trigonal bipyramidal geometry and zero for a perfect square pyramidal geometry. The crystal structure of the complex formed a 1D supramolecular chain by π···π interactions (Fig. 7). Strong π···π interactions were observed between the two imidazole rings (Cg(3): N1–C1–C6–N2–C7) of adjacent molecules, with a centroid–centroid separation of 3.6941(15) Å. In addition, strong interactions occur between the pyridyl (Cg(4): N3–C8–C9–C10–C11–C16) and phenyl rings (Cg(6): C1–C2–C3–C4–C5–C6) of two adjacent molecules, with a Cg–Cg distance of 3.7315(16) Å.

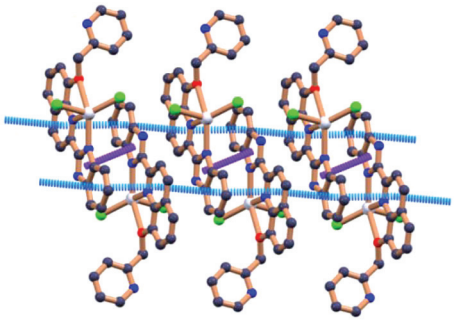

Fig. 7 1D-supramolecular structure formed by π···π interactions.

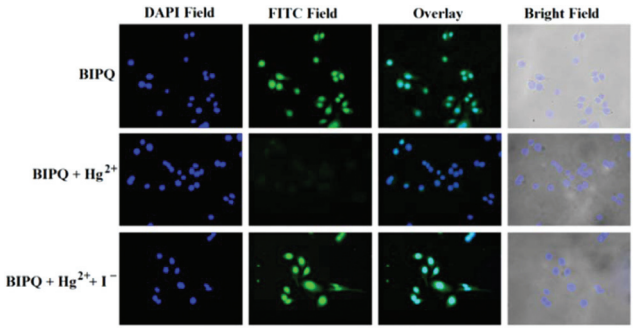

Fig. 9 Fluorescence images of AGS cells after incubation with BIPQ, BIPQ + Hg^{2+} and BIPQ + Hg^{2+} + I^- complex. DAPI was used to stain the nucleus; [BIPQ] = 15 μM, [Hg^{2+}] = 15 μM, [I^-] = 15 μM.

Cell study

The MTT experiment proved that the probe (BIPQ) has very trivial toxicity at lower concentration levels towards human gastric cancer (AGS) cells, although it has a prominently lower survivability effect of cells at a higher dosage (100 mM) (Fig. 8). Next, the IC_{50} value of the probe was calculated to be 185.1 μM; because the selected dose of the probe to be injected into the cell lines should be less than this IC_{50} value, we chose a 15 μM dosage to execute the experiment (ESI, Fig. S22†). The incubated cells exhibited strong fluorescence under a fluorescence microscope, which indicates that gastric cancer cells treated with free BIPQ display a clear, strong green fluorescence. In the presence of 15 μM Hg^{2+} along with the BIPQ, the intensity of the green fluorescence in the intracellular region is significantly diminished. Furthermore, when KI solution is added to the former solution, the green fluorescence intensity is once again noted inside the gastric cancer cells (Fig. 9). Further, the bright field images are the same as the images after incubation with Hg^{2+}; this signifies that the AGS cells are viable and that BIPQ is not at all toxic at that particular concentration. Thus, we can conclude that the probe BIPQ is a cell membrane-penetrable fluorescent switch that has potential applications in living cells for detecting Hg^{2+} and iodine.

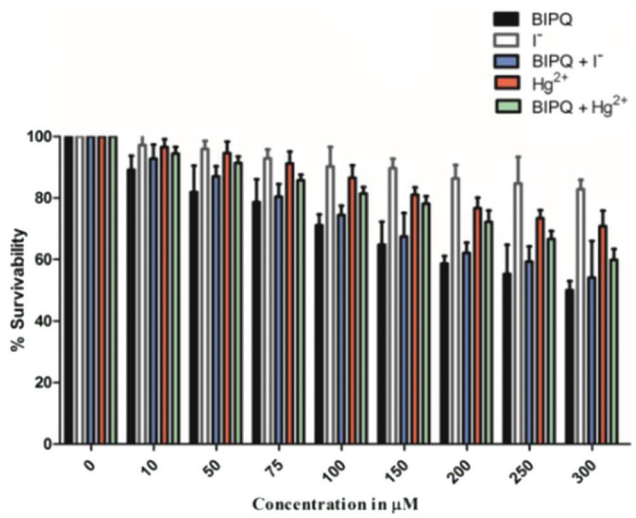

Fig. 8 MTT assay of BIPQ, Hg^{2+}, I^-, BIPQ + I^- and BIPQ + Hg^{2+} complex in the AGS cell line.

Conclusions

In summary, a new fluorescent reversible switch, BIPQ, was designed and developed for the fluorescence quenching of Hg^{2+} in aqueous media. It is noteworthy that this fluorescent "ON–OFF–ON" switch, BIPQ, exhibits remarkable emission quenching and shows a slight red-shift in its emission maximum at 485 nm on addition of increasing concentrations of Hg^{2+}. Moreover, this BIPQ-Hg^{2+} moiety can detect the presence of I^- selectively among other anions. The present fluorescent switch, BIPQ, shows high selectivity towards Hg^{2+} over other metal cations, with a sufficiently low detection limit on the order of 3.12×10^{-9} M in physiological conditions; meanwhile, the BIPQ-Hg^{2+} complex shows LOD values for I^- on the order of 5.48×10^{-8} M. To ascertain the complex formation of BIPQ with Hg^{2+}, single crystal X-ray studies were also performed along with ^1H and HRMS spectroscopy to assist the structural confirmation. Furthermore, due to its cell membrane penetrating power and low cytotoxic effect, the live cell imaging study of this new probe using a gastric cancer cell line (AGS) suggests that BIPQ can also be used as a bio-marker tool in the biological field.

Conflicts of interest

There are no conflicts to declare.

Acknowledgements

The authors thank the CSIR (No. 01(2992)/19/EMR-II) and SERB (No. EEQ/2018/000266), New Delhi, India for financial supports. K. A. thanks the Dr D. S. Kothari fellowship (UGC) (F.4-2/2006 (BSR)/CH/17-18/0224) for providing funding. S. G. and L. P. acknowledge UGC, New Delhi, India for providing fellowships.

Notes and references

1 C.-B. Huang, L. Xu, J.-L. Zhu, Y.-X. Wang, B. Sun, X. Li and H.-B. Yang, *J. Am. Chem. Soc.*, 2017, **139**, 9459.
2 Z. Xu, G. Li, Y.-Y. Ren, H. Huang, X. Wen, Q. Xu, X. Fan, Z. Huang, J. Huang and L. Xu, *Dalton Trans.*, 2016, **45**, 12087.
3 H.-I. Un, S. Wu, C.-B. Huang, Z. Xu and L. Xu, *Chem. Commun.*, 2015, **51**, 3143.
4 H.-I. Un, C.-B. Huang, J. Huang, C. Huang, T. Jia and L. Xu, *Chem. – Asian J.*, 2014, **9**, 3397.
5 L. Xu, Y. Xu, W. Zhu, B. Zeng, C. Yang, B. Wu and X. Qian, *Org. Biomol. Chem.*, 2011, **9**, 8284.
6 L. Xu, Y. Xu, W. Zhu, X. Sun, Z. Xu and X. Qian, *RSC Adv.*, 2012, **2**, 6323.
7 Environmental Protection Agency (EPA), *Fed. Regist.*, 2002, **9**, 1811.
8 M. Harada, *Crit. Rev. Toxicol.*, 1995, **25**, 1.
9 T. Zhang, B. Kim, C. Levard, B. C. Reinsch, G. V. Lowry, M. A. Deshusses and H. Hsu-Kim, *Environ. Sci. Technol.*, 2012, **46**, 6950.
10 J.-F. Chen, X.-B. Cheng, H. Li, B.-B. Han, Q. Lin, Y.-M. Zhang, H. Yao and T.-B. Wei, *New J. Chem.*, 2017, **41**, 12707.
11 K. Liu, Y. Zhang, T. Zhou, X. Liu, B. Chen, X. Wang, X. Zhao, J. Huo, Y. Wang and B. Zhu, *Sens. Actuators, B*, 2017, **253**, 1194.
12 V. Bhalla, R. Tejpal and M. Kumar, *Sens. Actuators, B*, 2010, **151**, 180.
13 A. K. Mahapatra, J. Roy, P. Sahoo, S. K. Mukhopadhyay and A. Chattopadhyay, *Org. Biomol. Chem.*, 2012, **10**, 2231.
14 G. Chen, Z. Guo, G. Zeng and L. Tang, *Analyst*, 2015, **140**, 5400.
15 H. N. Kim, W. X. Ren, J. S. Kim and J. Yoon, *Chem. Soc. Rev.*, 2012, **41**, 3210.
16 D. T. Quang and J. S. Kim, *Chem. Rev.*, 2010, **110**, 6280.
17 Q. Guo, Y. Zhang, Z.-H. Lin, Q.-Y. Cao and Y. Chen, *Dyes Pigm.*, 2020, **172**, 107872.
18 L.-N. Liu, H. Tao, G. Chen, Y. Chen and Q.-Y. Cao, *J. Lumin.*, 2018, **203**, 189.
19 P.-S. Yao, Z. Liu, J.-Z. Ge, Y. Chen and Q.-Y. Cao, *Dalton Trans.*, 2015, **44**, 7470.
20 A. Tang, Z. Chen, D. Deng, G. Liu, Y. Tu and S. Pu, *RSC Adv.*, 2019, **9**, 11865.
21 Y.-Y. Guo, X.-L. Tang, F.-P. Hou, J. Wu, W. Dou, W.-W. Qin, J.-X. Ru, G.-L. Zhang, W.-S. Liu and X.-J. Yao, *Sens. Actuators, B*, 2013, **181**, 202.
22 H. Mohammad, A. S. M. Islam, C. Prodhan and M. Ali, *New J. Chem.*, 2019, **43**, 5297.
23 K. C. Song, J. S. Kim, S. M. Park, K.-C. Chung, S. Ahn and S.-K. Chang, *Org. Lett.*, 2006, **8**, 3413.
24 G. Yang, X. Meng, S. Fang, H. Duan, L. Wang and Z. Wang, *RSC Adv.*, 2019, **9**, 8529.
25 K. Silpcharu, M. Sukwattanasinitta and P. Rashatasakhon, *RSC Adv.*, 2019, **9**, 11451.
26 K. Tsukamoto, Y. Shinohara, S. Iwasaki and H. Maeda, *Chem. Commun.*, 2011, **47**, 5073.
27 G. G. V. Kumar, R. S. Kannan, T. C.-K. Yang, J. Rajesh and G. Sivaraman, *Anal. Methods*, 2019, **11**, 901.
28 G. Aumont and J.-C. Tressol, *Analyst*, 1986, **111**, 841.
29 M. Haldimann, B. Zimmerli, C. Als and H. Gerber, *Clin. Chem.*, 1998, **44**, 817.
30 K. Markou, N. Georgopoulos, V. Kyriazopoulou and A. G. Vagenakis, *Thyroid*, 2011, **11**, 501.
31 J. T. Dunn, *Ann. Inst. Biol. (Tihany)*, 1993, **678**, 158.
32 A. Stagnaro-Green and E. Pearce, *Nat. Rev. Endocrinol.*, 2012, **8**, 650.
33 F. Delange, C. Thilly and A. M. Ermans, *J. Clin. Endocrinol. Metab.*, 1968, **28**, 114.
34 B. S. Hetzel, *J. Nutr.*, 2000, **130**, 493.
35 F. Delange, *Postgrad. Med. J.*, 2001, **77**, 217.
36 F. Soriguer, C. Gutiérrez-Repiso, E. Rubio-Martin, F. Linares, I. Cardona, J. López-Ojeda, M. Pacheco, S. González-Romero, M. J. Garriga, I. elasco, P. Santiago and E. García-Fuentes, *J. Nutr.*, 2011, **105**, 1783.
37 H.-I. Un, C.-B. Huang, C. Huang, T. Jia, X.-L. Zhao, C.-H. Wang, L. Xu and H.-B. Yang, *Org. Chem. Front.*, 2014, **1**, 1083.
38 S. Ozturk and S. Atilgan, *Tetrahedron Lett.*, 2014, **55**, 70.
39 M. Dong, Y.-W. Wang and Y. Peng, *Org. Lett.*, 2010, **12**, 5310.
40 M. Sohrabi, M. Amirnasr, S. Meghdadi, M. Lutz, M. B. Torbati and H. Farrokhpour, *New J. Chem.*, 2018, **42**, 12595.
41 G. Yang, X. Meng, S. Fang, L. Wang, Z. Wang, F. Wang, H. Duan and A. Hao, *New J. Chem.*, 2018, **42**, 14630.
42 A. O. Eseola, H. Görls, M. Bangesh and W. Plass, *New J. Chem.*, 2018, **42**, 7884.
43 M. A. Hossain, S. O. Kang, J. M. Llinares, D. Powell and K. Bowman-James, *Inorg. Chem.*, 2003, **42**, 1397.
44 E. J. O'Neil and B. D. Smith, *Coord. Chem. Rev.*, 2006, **250**, 3068.
45 N. Singh and D. O. Jang, *Org. Lett.*, 2007, **9**, 1991.
46 L.-R. Lin, W. Fang, Y. Yu, R.-B. Huang and L.-S. Zheng, *Spectrochim. Acta, Part A*, 2007, **67**, 1403.
47 H. Kim and J. Kang, *Tetrahedron Lett.*, 2005, **46**, 5443.
48 R. Martínez-Máñez and F. Sancenón, *Chem. Rev.*, 2003, **103**, 4419.
49 C. Lin, V. Simov and D. G. Drueckhammer, *J. Org. Chem.*, 2007, **72**, 1742.
50 C. Caltagirone and P. A. Gale, *Chem. Soc. Rev.*, 2009, **38**, 520.
51 P. A. Gale and C. Caltagirone, *Coord. Chem. Rev.*, 2018, **354**, 2.
52 P. A. Gale, E. N. W. Howe and X. Wu, *Chem*, 2016, **1**, 351.
53 F. M. Pfeffer, M. Seter, N. Lewcenko and N. W. Barnett, *Tetrahedron Lett.*, 2006, **47**, 5241.
54 M. J. Frisch, G. W. Trucks, H. B. Schlegel, G. E. Scuseria, M. A. Robb, J. R. Cheeseman, G. Scalmani, V. Barone, B. Mennucci, G. A. Petersson, H. Nakatsuji, M. Caricato, X. Li, H. P. Hratchian, A. F. Izmaylov, J. Bloino, G. Zheng, J. L. Sonnenberg, M. Hada, M. Ehara, K. Toyota, R. Fukuda, J. Hasegawa, M. Ishida, T. Nakajima, Y. Honda, O. Kitao, H. Nakai, T. Vreven, J. A. Montgomery Jr., J. E. Peralta,

F. Ogliaro, M. Bearpark, J. J. Heyd, E. Brothers, K. N. Kudin, V. N. Staroverov, R. Kobayashi, J. Normand, K. Raghavachari, A. Rendell, J. C. Burant, S. S. Iyengar, J. Tomasi, M. Cossi, N. Rega, J. M. Millam, M. Klene, J. E. Knox, J. B. Cross, V. Bakken, C. Adamo, J. Jaramillo, R. Gomperts, R. E. Stratmann, O. Yazyev, A. J. Austin, R. Cammi, C. Pomelli, J. W. Ochterski, R. L. Martin, K. Morokuma, V. G. Zakrzewski, G. A. Voth, P. Salvador, J. J. Dannenberg, S. Dapprich, A. D. Daniels, Ö. Farkas, J. B. Foresman, J. V. Ortiz, J. Cioslowski and D. J. Fox, *Gaussian 09, Revision D.01*, Gaussian, Inc., Wallingford, CT, 2009.

55 A. D. Becke, *J. Chem. Phys.*, 1993, **98**, 5648.

56 C. Lee, W. Yang and R. G. Parr, *Phys. Rev. B: Condens. Matter Mater. Phys.*, 1988, **37**, 785.

57 P. J. Hay and W. R. Wadt, *J. Chem. Phys.*, 1985, **82**, 299.

58 R. Bauernschmitt and R. Ahlrichs, *Chem. Phys. Lett.*, 1996, **256**, 454.

59 R. E. Stratmann, G. E. Scuseria and M. J. Frisch, *J. Chem. Phys.*, 1998, **109**, 8218.

60 M. E. Casida, C. Jamorski, K. C. Casida and D. R. Salahub, *J. Chem. Phys.*, 1998, **108**, 4439.

61 V. Barone and M. Cossi, *J. Phys. Chem. A*, 1998, **102**, 1995.

62 M. Cossi and V. Barone, *J. Chem. Phys.*, 2001, **115**, 4708.

63 M. Cossi, N. Rega, G. Scalmani and V. Barone, *J. Comput. Chem.*, 2003, **24**, 669.